doi:10.3772/j.issn.1006-6748.2021.03.010

Networked guaranteed cost PID attitude tracking control of a laboratory flight system①

Liu Yicai (刘义才)②*,**, Liu Bin*

(*Engineering Research Center for Metallurgical Automation and Detecting Technology of Ministry of Education, Institute of Information Science and Engineering, Wuhan University of Science and Technology, Wuhan 430081, P. R. China)

(**School of Mechanical-Electronic and Automobile Engineering, Wuhan Business University, Wuhan 430056, P. R. China)

Abstract

This paper investigates the networked flight control system for a laboratory 3 degrees of freedom (3-DOF) helicopter, and presents a novel networked guaranteed cost proportion-integration-differentiation (PID) attitude tracking control method with consideration of time-varying delay and packet dropouts. As the 3-DOF helicopter characteristics of multi-input multi-output (MIMO), channel coupling, and nonlinearity, a genera linear time delay system is modeled by analyzing the motions on elevation, pitch, and travel axis. By using the reciprocal convex approach, the free weight matrix, and the cone complementarity linearization (CCL) method, the PID tracking controller parameters can be designed if the related linear matrix inequalities (LMIs) are feasible. Finally, a practical experiment of laboratory 3-DOF helicopter is given, and the experimental results show that the proposed method is effective.

Key words: time-varying delay, packet dropout, networked flight control system, tracking control

0 Introduction

The laboratory 3 degrees of freedom (3-DOF) helicopter, acting as a good experimental platform for aerial vehicles controller, has attracted wide attention[1-3]. It is the abstraction of aerial vehicles systems, which maintains similar actuator, sensor, and driving principle. In 3-DOF helicopter, there are many important characteristics such as multi-input multi-output (MIMO), nonlinearity, coupling. Therefore, it plays a very good role in verifying the control algorithm. In recent years, the considerable attention has been given to the analysis and control of helicopters. For instance, the attitude tracking problem for a 3-DOF laboratory helicopter has been addressed by robust control approach in Refs[4,5]. In addition, model predictive control[6], sliding mode control[7-8], nonlinear control method[9-10], fuzzy control technique[11], back stepping-based approach[12], and H∞ control mechanism[13] have been used to track the desired references for helicopters. Unfortunately, all the methods mentioned above have been proved to be effective but only limited to the local control. The information interaction between the aerial vehicles and the ground control center is a prerequisite for the remote control. Therefore, the 3-DOF unmanned flight system is a typical networked control system (NCS)[14-15]. However, the communication network between them will be affected by factors such as weather, electromagnetic interference, network congestion, intermittent failure of communication equipment and so on, which inevitably leads to non-ideal network quality of services (QoS), e.g., network-induced delays, data packet dropouts. These will make the analysis and synthesis of 3-DOF helicopter more complex[16-17]. To the best of the authors' knowledge, the problem of networked tracking control for a 3-DOF helicopter has not been investigated and still remains challenging, which motivates the present study.

Although many advanced control theories and practical design techniques have been proposed, most control loops are still proportion-integration-differentiation (PID) with a wide range of applications[18]. Recently networked PID control methods have also developed. For instance, by gain and phase margins approach, Ref. [19] proposed a novel normalized PI/PID controller for NCSs based on analyzing the stability

① Supported by the National Natural Science Foundation of China (No. 61573263).

② To whom correspondence should be addressed. E-mail: liuyicai027@wbu.edu.cn

Received on Aug. 31, 2020

and robustness of system under the effect of network-induced delays. In Ref. [20], speed senseless and sensor-fault tolerant optimal PI regulator for networked DC motor system with unknown time-delay and packet dropouts was presented based on bilinear matrix inequality. In Refs[21,22], by using a novel technique, PID controllers were converted into output feedback controllers. However, the helicopter flight control system is a typical MIMO high order system, and has strong channel coupling and nonlinear characteristics. The mentioned networked PID methods are difficult to apply directly to the trajectory tracking control.

Inspired by the above, the modeling of 3-DOF helicopter and the networked PID tracking control are investigated in this paper, and a networked guaranteed cost PID controller to achieve attitude tracking control of a 3-DOF helicopter under network constraints (network-induced time-varying delays, data packet dropouts) is designed. The main contributions of this paper can be identified as follows. (1) Network-induced delays and data packet dropouts are taken into account, and the 3-DOF helicopter is modeled as a time delay system. (2) A systematic networked PID design method with the NCSs structure is presented.

1 Modeling of 3-DOF helicopter

The 3-DOF laboratory helicopter from Quanser Consulting Inc. (see Fig. 1) acts as an ideal experimental platform. As described in Fig. 2, the 3-DOF laboratory helicopter refers to the motion of elevation, pitch, and travel axis.

Fig. 1 The 3-DOF laboratory helicopter platform

As shown in Fig. 1 and Fig. 2, the two DC motors, known as the front motor and the back motor, are installed at the end of the helicopter frame respectively to drive two propellers. The helicopter attitude is controlled by the thrust forces F_b and F_f which are generated by two propellers. A positive voltage applied to the front motor causes a positive pitch while a negative voltage applied to the back motor causes a negative pitch. A positive voltage to either motor also causes an elevation of the body. If the body pitches, the thrust vectors result in a travel of the body as well.

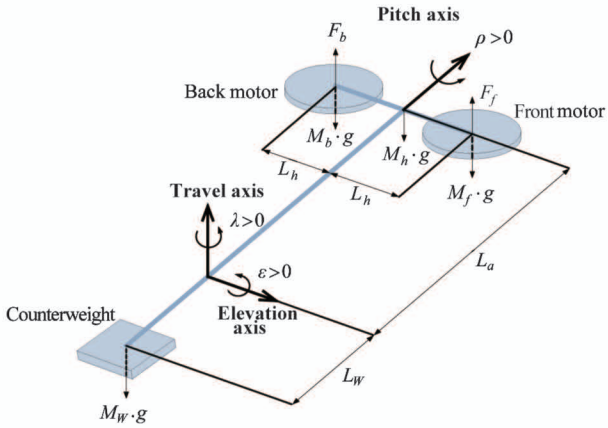

Fig. 2 The free-body diagram of 3-DOF helicopter

At the other end of the arm, it carries a counterweight, which makes the effective mass of the helicopter light enough to be lifted using the thrust from the motors. The thrust forces acting on the elevation, pitch, and travel axis from the front and back motors are defined and made relative to the quiescent voltage or operating point.

$$V_{op} = \frac{1}{2}\frac{g(L_w m_w - L_a m_f - L_a m_b)}{L_a K_f} \tag{1}$$

Obviously, the helicopter has only 2 control inputs, namely, front voltage and back voltage, whereas it contains 3 outputs, that is, pitch, elevation, and travel angles. The aim of this paper is to design networked guaranteed cost PID tracking control system to regulate and track the elevation and travel angles of the 3-DOF helicopter. In order to obtain the linear 3-DOF state space model, the physical parameter values are considered as shown in Table 1, which are obtained from the Quanser helicopter laboratory and user manual.

1.1 The dynamics model of elevation axis

Taking into account the motion on elevation axis as shown in Fig. 3, it can be concluded that the motion is determined by the torque, which is generated by $F_s = F_f + F_b$. Considering the actual movement of a helicopter, the varying of pitch and elevation are small, thus $\cos(\rho) \approx 1$ and $\cos(\varepsilon) \approx 1$ can be obtained, and the Eq. (2) can be formulated based on the quiescent voltage V_{op}.

$$J_\varepsilon \ddot{\varepsilon} = (F_f + F_b)\cos(\rho)L_a - T_g\cos(\varepsilon) \approx K_f(U_f + U_b)L_a \quad (2)$$

where ρ is the elevation angular, ε is the elevation angular, $\ddot{\varepsilon}$ is the elevation angular acceleration, the forces F_f and F_b are obtained by the control voltages U_f and U_b, respectively. $J_\varepsilon = m_f L_a^2 + m_a L_a^2 + m_w L_w^2 = m_t L_a^2 + m_w L_w^2$ is the elevation rotary inertia.

Table 1 Parameters of the 3-DOF helicopter platform

Parameter	K_f	L_a	L_w	L_h
Definition	Propeller force-thrust constant	Distance between travel axis and helicopter body	Distance between travel axis and the counterweight	Distance between pitch axis and each motor
Value	0.1188 N/V	0.660 m	0.470 m	0.178 m
Parameter	T_g	m_t	m_f, m_b	m_w
Definition	Effective gravity on elevation axis	Total mass of two propeller assemblies	Mass of front/back propeller assemblies	Mass of the counterweight
Value	$T_g = m_t g L_a - m_w g L_w$	$m_t = m_f + m_b$	0.713 kg	1.87 kg

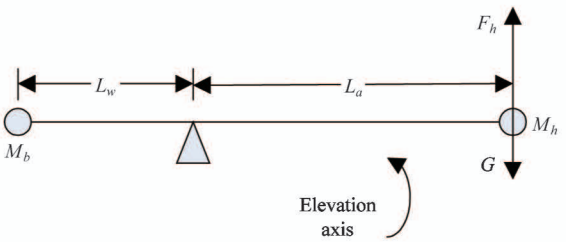

Fig. 3 Schematic diagram for elevation

Let $m_t = m_f + m_b$, the linear expression Eq. (3) of the elevation angular acceleration can be obtained.

$$\ddot{\varepsilon} = \frac{K_f L_a (U_f + U_b)}{m_t L_a^2 + m_w L_w^2} = \frac{K_f L_a V_s}{m_t L_a^2 + m_w L_w^2} \quad (3)$$

1.2 The dynamics model of pitch axis

Considering the motion on pitch axis as shown in Fig. 4, it can be inferred that the motion is caused by the pitch rotary inertia, which is generated by $F_d = F_f - F_b$. Therefore, the dynamics model Eq. (4) of pitch axis can be established.

$$J_p \ddot{\rho} = (F_f - F_b)L_h = K_f(U_f - U_b)L_h \quad (4)$$

where $\ddot{\rho}$ is the pitch angular acceleration, $J_p = 2m_f L_h^2$ is the pitch rotary inertia. Then there is

$$\ddot{\rho} = \frac{K_f(U_f - U_b)L_h}{2m_f L_h^2} = \frac{K_f V_d L_h}{2m_f L_h^2} \quad (5)$$

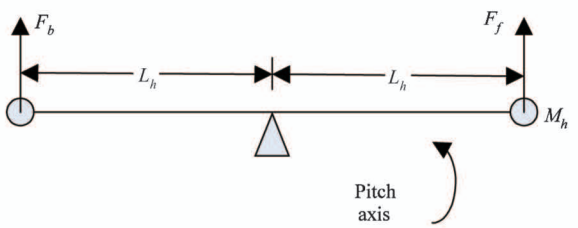

Fig. 4 Schematic diagram for pitch

1.3 The dynamics model of travel axis

When the pitch axis is tilted, the horizontal component of thrust forces $F_g\sin(\rho)$ will cause a torque about the travel axis, which results in an acceleration about the travel axis. Assume the body pitches by an angle ρ as shown in Fig. 5. The dynamics model of travel axis can be described as

$$J_\lambda \ddot{\lambda} = L_a F_g \sin(\rho) = L_a(F_f + F_b)\sin(\rho) = L_a K_f(U_f + U_b)\sin(\rho) \quad (6)$$

where λ is travel angular, $\ddot{\lambda}$ is travel angular acceleration, $J_\lambda = m_f L_f^2 + m_b L_b^2 + m_w L_w^2$ is travel rotary inertia, and $L_f^2 = L_b^2 = L_h^2 + L_a^2$.

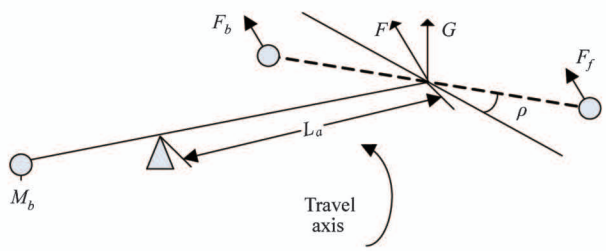

Fig. 5 Schematic diagram for travel

$F_g\cos(\rho)$ is the required force to maintain the helicopter body pitches by an angle ρ. Hypothesizing the pitch angle ρ is small, $\sin(\rho) \approx \rho$ and $\cos(\rho) \approx 1$. Thus $\ddot{\lambda}$ can be described approximately as

$$\ddot{\lambda} \approx -\frac{T_g \rho}{2m_f L_h^2 + 2m_f L_a^2 + m_w L_w^2} \quad (7)$$

Define

$$\boldsymbol{x}(t) = \left[\varepsilon \quad \rho \quad \lambda \quad \frac{\mathrm{d}}{\mathrm{d}t}\varepsilon \quad \frac{\mathrm{d}}{\mathrm{d}t}\rho \quad \frac{\mathrm{d}}{\mathrm{d}t}\lambda \quad \int \varepsilon \mathrm{d}t \quad \int \lambda \mathrm{d}t\right]^{\mathrm{T}},$$

$\boldsymbol{u}(t) = [U_f \quad U_b]^{\mathrm{T}}$, $\boldsymbol{y}(t) = [\varepsilon \quad \rho \quad \lambda]^{\mathrm{T}}$. According to Eq. (3), Eq. (5) and Eq. (7), the linear state space representation for the 3-DOF helicopter system can be modeled as

$$\begin{cases} \dot{\boldsymbol{x}}(t) = \boldsymbol{A}\boldsymbol{x}(t) + \boldsymbol{B}\boldsymbol{u}(t) \\ \boldsymbol{y}(t) = \boldsymbol{C}\boldsymbol{x}(t) \end{cases} \quad (8)$$

where $\boldsymbol{A}$ =

$$\begin{bmatrix} 0 & 0 & 0 & 1 & 0 & 0 & 0 & 0 \\ 0 & 0 & 0 & 0 & 1 & 0 & 0 & 0 \\ 0 & 0 & 0 & 0 & 0 & 1 & 0 & 0 \\ 0 & 0 & 0 & 0 & 0 & 0 & 0 & 0 \\ 0 & 0 & 0 & 0 & 0 & 0 & 0 & 0 \\ 0 & -\dfrac{(L_w m_w - 2L_a m_f)g}{2m_f L_h^2 + 2m_f L_a^2 + m_w L_w^2} & 0 & 0 & 0 & 0 & 0 & 0 \\ 1 & 0 & 0 & 0 & 0 & 0 & 0 & 0 \\ 0 & 0 & 1 & 0 & 0 & 0 & 0 & 0 \end{bmatrix},$$

$$\boldsymbol{B} = \begin{bmatrix} 0 & 0 \\ 0 & 0 \\ 0 & 0 \\ \dfrac{L_a K_f}{2m_f L_a^2 + m_w L_w^2} & \dfrac{L_a K_f}{2m_f L_a^2 + m_w L_w^2} \\ \dfrac{1}{2}\dfrac{K_f}{m_f L_h} & -\dfrac{1}{2}\dfrac{K_f}{m_f L_h} \\ 0 & 0 \\ 0 & 0 \\ 0 & 0 \end{bmatrix},$$

$$\boldsymbol{C} = \begin{bmatrix} 1 & 0 & 0 & 0 & 0 & 0 & 0 & 0 \\ 0 & 1 & 0 & 0 & 0 & 0 & 0 & 0 \\ 0 & 0 & 1 & 0 & 0 & 0 & 0 & 0 \end{bmatrix},$$

$$\boldsymbol{K} = \begin{bmatrix} k_{11} & k_{12} & k_{13} & k_{14} & k_{15} & k_{16} & k_{17} & k_{18} \\ k_{21} & k_{22} & k_{23} & k_{24} & k_{25} & k_{26} & k_{27} & k_{28} \end{bmatrix},$$

$$\boldsymbol{u}(t) = \begin{bmatrix} U_f \\ U_b \end{bmatrix} = \boldsymbol{K}\boldsymbol{x}(t).$$

Obviously, it can be seen from the dynamic Eqs (2) – (7) that the 3-DOF helicopter is a typical MIMO model, which has 2 input variables U_f and U_b, and 3 output variables ρ, ε and λ. Therefore, the 3-DOF helicopter is under-actuated. And the outputs of the 3 channels are coupling. For instance, the pitch angle ρ is coupled in the elevation equation, and ρ also affects the travel λ in the travel axis equation. Only when the range of pitching angle ρ and elevation angle ε is very small at the same time, the proposed method could be used to obtain the linearized state Eq. (8). However, the actual 3-DOF helicopter is still a typical system with strong coupling, MIMO, and nonlinear.

As shown in Fig. 6, the 3-DOF helicopter as the controlled plant is assembled in the network. Therefore, it is a typical networked control system architecture. Before further proceeding, the following assumptions are made, which are common in NCSs research.

Assume 1 h is the sampling period of the sensor, and $i_k h$, $i_k \in N$ is sampling instant.

Assume 2 The zero-order-hold (ZOH) is used to hold the control input when there is no latest control packet arriving at the actuator.

Assume 3 Define $\tau_k = \tau_k^{sc} + \tau_k^{ca}$, where τ_k^{sc} and τ_k^{ca} represent network-induced time-varying delays which exist in sensor-to-controller and controller-to-actuator channel, respectively. The maximum number d of consecutive packet dropouts in NCSs has an upper bound $\bar{d}$.

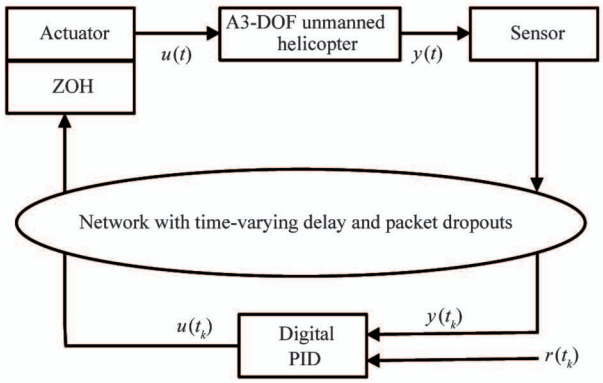

Fig. 6 The schematic of networked tracking control for a 3-DOF helicopter

Considering the network-induced delays and packet dropouts which exist in the communication channels, the holding interval of the ZOH is $[\, i_k h + \tau_k \quad i_k h + (d+1)h + \tau_{k+1})$. By defining $\tau(t) = t - i_k h$, $\underline{\tau} = \tau_m \leqslant \tau(t) \leqslant (\bar{d}+1)h + \tau_M = \bar{\tau}$ can be obtained, where τ_M and τ_m represent maximum and minimum network-induced time-varying delay τ_k, respectively. Obviously $\tau(t)$ is piecewise-linear with the first derivative satisfying $\dot{\tau}(t) = 1$. This characteristic will be taken into consideration to reduce the analysis and design conservativeness in next section.

Considering the holding interval of the ZOH, the state feedback control law can be expressed as

$$\boldsymbol{u}(t) = \boldsymbol{K}\boldsymbol{x}(t_k h) = \boldsymbol{K}(\boldsymbol{x}(t - \tau(t))) \qquad t \in [\, t_k h + \tau_k, \quad t_{k+1} h + \tau_{k+1})$$

where $t_k \in \{i_k\}$ represents the data sampling instant, and the sampled data is transmitted successfully from sensor to actuator. Therefore, the closed-loop NCS can be obtained as

$$\begin{cases} \dot{\boldsymbol{x}}(t) = \boldsymbol{A}\boldsymbol{x}(t) + \boldsymbol{B}\boldsymbol{K}\boldsymbol{x}(t - \tau(t)) \\ \qquad\qquad t \in [\, t_k h + \tau_k, \, t_{k+1} h + \tau_{k+1}) \\ \boldsymbol{y}(t) = \boldsymbol{C}\boldsymbol{x}(t) \end{cases} \tag{9}$$

The feedback control gain for this system are calculated by using a linear quadratic regulation (LQR) approach with the given positive diagonal $\hat{\boldsymbol{Q}}$ and $\hat{\boldsymbol{R}}$ matrices. The quadratic cost function is defined as

$$J = \int_0^\infty (\boldsymbol{x}^{\mathrm{T}}(t)\hat{\boldsymbol{Q}}\boldsymbol{x}(t) + \boldsymbol{u}^{\mathrm{T}}(t)\hat{\boldsymbol{R}}\boldsymbol{u}(t))\,\mathrm{d}t$$

Definition 1 Considering the 3-DOF helicopter system Eq. (8), if there exist a control law $\boldsymbol{u}^*(t)$ =

$\boldsymbol{Kx}(t)$ and a positive scalar J^* such that the NCS Eq. (9) is stable and the value of the cost function satisfies $J \leqslant J^*$, then J^* is said to be a guaranteed cost and $\boldsymbol{u}^*(t)$ is said to be a guaranteed cost control law for the system Eq. (9).

The purpose of this paper is to realize the networked PID tracking control for a 3-DOF helicopter with the LQR approach and make the cost function or performance index J have an upper bound.

2 Main results

In this section, by applying a new Lyapunov-Krasovskii functional, the tuning of PID is converted into the solution of matrix inequalities. Then the linear matrix inequality (LMI) stability conditions and controller design for closed-loop system Eq. (9) will be established in this section.

2.1 PID control equation

If ε_d, ρ_d, and λ_d are the desired elevation angle, desired pitch angle and desired travel angle of 3-DOF helicopter system, the PID controller parameters will be designed in the following form to meet system expectations, PID for elevation axis:

$$V_s = k_{\varepsilon p}\varepsilon_e + k_{\varepsilon d}\dot{\varepsilon}_e + k_{\varepsilon i}\int \varepsilon_e \mathrm{d}t$$

PD for pitch axis:

$$V_d = K_{\rho p}(\rho - \rho_d) + K_{\rho d}\dot{\rho}$$

and PID for travel axis:

$$\rho_d = k_{\lambda p}\lambda_e + k_{\lambda d}\dot{\lambda}_e + k_{\lambda i}\int \lambda_e \mathrm{d}t$$

where $k_{\varepsilon p}$, $k_{\varepsilon d}$, $k_{\varepsilon i}$, $k_{\rho p}$, $k_{\rho d}$, $k_{\lambda p}$, $k_{\lambda d}$ and $k_{\lambda i}$ are the elements of the control gain K, and $\varepsilon_e = \varepsilon - \varepsilon_d$, $\lambda_e = \lambda - \lambda_d$.

2.2 LMI stability condition for networked PID control

Lemma 1[23] Let $f_1, f_2, \cdots, f_N: \Re^m \to \Re$ have positive values in an open subset D of $\Re^m$. Then, the reciprocally convex combination of f_i over D satisfies:

$$\min_{\{\beta_i | \beta_i > 0,\ \sum_i \beta_i = 1\}} \sum_i \frac{1}{\beta_i} f_i(t) = \sum_i f_i(t) + \max_{g_{i,j}} \sum_{i \neq j} g_{i,j}(t)$$

subject to $g_{i,j}: \Re^m \to \Re$, $g_{i,j}(t) = g_{j,i}(t)$, $\begin{bmatrix} f_i(t) & g_{j,i}(t) \\ g_{i,j}(t & f_j(t) \end{bmatrix} \geqslant 0$.

Lemma 2[24] $\boldsymbol{\Xi}_i (i = 1, 2)$ and $\boldsymbol{\Omega}$ are matrices with appropriate dimensions, $\eta(t)$ is a function of t and $\underline{\eta} \leqslant \eta(t) \leqslant \bar{\eta}$, then $\eta(t)\boldsymbol{\Xi}_1 + (\bar{\eta} - \eta(t))\boldsymbol{\Xi}_2 + \boldsymbol{\Omega} < 0$ if and only if $\bar{\eta}\boldsymbol{\Xi}_2 + \boldsymbol{\Omega} \leqslant 0$ and $\underline{\eta}\boldsymbol{\Xi}_1 + (\bar{\eta} - \underline{\eta})\boldsymbol{\Xi}_2 + \boldsymbol{\Omega} < 0$.

Theorem 1 For given scalars $0 < \underline{\tau} < \bar{\tau}$, and a gain $\boldsymbol{K}$, the closed-loop NCS Eq. (9) is asymptotically stable, and the upper bound of cost function or performance index J is minimized, if there exist matrices $\boldsymbol{X} > 0$, $\boldsymbol{Y} > 0$, $\boldsymbol{Q}_1 > 0$, $\boldsymbol{Q}_2 > 0$, $\boldsymbol{R}_1 > 0$, $\boldsymbol{R}_2 > 0$, $\boldsymbol{H} > 0$, $\boldsymbol{M}$ and $\boldsymbol{U}$ with appropriate dimensions such that

$$\begin{bmatrix} \boldsymbol{R}_2 & * \\ \boldsymbol{U} & \boldsymbol{R}_2 \end{bmatrix} > 0 \tag{10}$$

$$\begin{aligned} \boldsymbol{\Xi}_1 = & \left(\boldsymbol{\Xi} + \underline{\tau}\boldsymbol{M}\boldsymbol{H}^{-1}\boldsymbol{M}^{\mathrm{T}} + \boldsymbol{M}(\boldsymbol{e}_1 - \boldsymbol{e}_3) \right. \\ & \left. + (\boldsymbol{e}_1 - \boldsymbol{e}_3)^{\mathrm{T}}\boldsymbol{M}^{\mathrm{T}} + (\bar{\tau} - \underline{\tau})\boldsymbol{\Gamma}^{\mathrm{T}}\boldsymbol{H}\boldsymbol{\Gamma} \right) \\ & + \boldsymbol{e}_1^{\mathrm{T}}(\hat{\boldsymbol{Q}} + \boldsymbol{K}^{\mathrm{T}}\hat{\boldsymbol{R}}\boldsymbol{K})\boldsymbol{e}_1 \leqslant 0 \end{aligned} \tag{11}$$

$$\begin{aligned} \boldsymbol{\Xi}_2 = & \left(\boldsymbol{\Xi} + \bar{\tau}\boldsymbol{M}\boldsymbol{H}^{-1}\boldsymbol{M}^{\mathrm{T}} + \boldsymbol{M}(\boldsymbol{e}_1 - \boldsymbol{e}_3) \right. \\ & \left. + (\boldsymbol{e}_1 - \boldsymbol{e}_3)^{\mathrm{T}}\boldsymbol{M}^{\mathrm{T}} \right) \\ & + \boldsymbol{e}_1^{\mathrm{T}}(\hat{\boldsymbol{Q}} + \boldsymbol{K}^{\mathrm{T}}\hat{\boldsymbol{R}}\boldsymbol{K})\boldsymbol{e}_1 \leqslant 0 \end{aligned} \tag{12}$$

where $\boldsymbol{M} = [\boldsymbol{M}_1^{\mathrm{T}} \ \boldsymbol{M}_2^{\mathrm{T}} \ \boldsymbol{M}_3^{\mathrm{T}} \ \boldsymbol{M}_4^{\mathrm{T}} \ \boldsymbol{M}_5^{\mathrm{T}}]^{\mathrm{T}}$,

$\boldsymbol{e}_1 = [\boldsymbol{I} \ 0 \ 0 \ 0]$, $\boldsymbol{e}_3 = [0 \ 0 \ \boldsymbol{I} \ 0]$,

$$\boldsymbol{\Xi} = \begin{bmatrix} \boldsymbol{\Xi}_{11} & * & * & * \\ \boldsymbol{\Xi}_{21} & \boldsymbol{\Xi}_{22} & * & * \\ \boldsymbol{\Xi}_{31} & \boldsymbol{\Xi}_{32} & \boldsymbol{\Xi}_{33} & * \\ 0 & \boldsymbol{\Xi}_{42} & \boldsymbol{\Xi}_{43} & \boldsymbol{\Xi}_{44} \end{bmatrix}, \ \boldsymbol{\Gamma} = [\boldsymbol{A} \ \ 0 \ \ \boldsymbol{B}\boldsymbol{K} \ \ 0],$$

$$\begin{aligned} \boldsymbol{\Xi}_{11} &= \boldsymbol{A}^{\mathrm{T}}\boldsymbol{P} + \boldsymbol{P}\boldsymbol{A} + \boldsymbol{Q}_1 + \underline{\tau}^2\boldsymbol{A}^{\mathrm{T}}\boldsymbol{R}_1\boldsymbol{A} + (\bar{\tau} - \underline{\tau})^2\boldsymbol{A}^{\mathrm{T}}\boldsymbol{R}_2\boldsymbol{A} \\ &\quad - \boldsymbol{R}_1, \ \boldsymbol{\Xi}_{21} = \boldsymbol{R}_1, \\ \boldsymbol{\Xi}_{22} &= \boldsymbol{Q}_2 - \boldsymbol{Q}_1 - \boldsymbol{R}_1 - \boldsymbol{R}_2, \\ \boldsymbol{\Xi}_{31} &= \boldsymbol{K}^{\mathrm{T}}\boldsymbol{B}^{\mathrm{T}}\boldsymbol{P} + \underline{\tau}^2\boldsymbol{K}^{\mathrm{T}}\boldsymbol{B}^{\mathrm{T}}\boldsymbol{R}_1\boldsymbol{A} + (\bar{\tau} - \underline{\tau})^2\boldsymbol{K}^{\mathrm{T}}\boldsymbol{B}^{\mathrm{T}}\boldsymbol{R}_2\boldsymbol{A}, \\ \boldsymbol{\Xi}_{32} &= -\boldsymbol{U} + \boldsymbol{R}_2, \\ \boldsymbol{\Xi}_{33} &= \underline{\tau}^2\boldsymbol{K}^{\mathrm{T}}\boldsymbol{B}^{\mathrm{T}}\boldsymbol{R}_1\boldsymbol{B}\boldsymbol{K} + (\bar{\tau} - \underline{\tau})^2\boldsymbol{K}^{\mathrm{T}}\boldsymbol{B}^{\mathrm{T}}\boldsymbol{R}_2\boldsymbol{B}\boldsymbol{K} \\ &\quad - (2\boldsymbol{R}_2 - \boldsymbol{U}^{\mathrm{T}} - \boldsymbol{U}), \\ \boldsymbol{\Xi}_{42} &= \boldsymbol{U}, \ \boldsymbol{\Xi}_{43} = -\boldsymbol{U} + \boldsymbol{R}_2, \ \boldsymbol{\Xi}_{44} = -\boldsymbol{Q}_2 - \boldsymbol{R}_2. \end{aligned}$$

Poof Construct a Lyapunov-Krasovskii functional candidate as

$$V(t) = \sum_{i=1}^{3} V_i(t, \boldsymbol{x}_t), \ t \in [t_k h + \tau_k, \ t_{k+1}h + \tau_{k+1}),$$

where $V_1(t, \boldsymbol{x}_t) = \boldsymbol{x}^{\mathrm{T}}(t)\boldsymbol{P}\boldsymbol{x}(t)$,

$$V_2(t, \boldsymbol{x}_t) = \int_{t-\underline{\tau}}^{t} \dot{\boldsymbol{x}}^{\mathrm{T}}(s)\boldsymbol{Q}_1\dot{\boldsymbol{x}}(s)\mathrm{d}s + \int_{t-\bar{\tau}}^{t-\underline{\tau}} \dot{\boldsymbol{x}}^{\mathrm{T}}(s)\boldsymbol{Q}_2\dot{\boldsymbol{x}}(s)\mathrm{d}s,$$

$$\begin{aligned} V_3(t, \boldsymbol{x}_t) &= \underline{\tau}\int_{t-\underline{\tau}}^{t}\int_{s}^{t} \dot{\boldsymbol{x}}^{\mathrm{T}}(v)\boldsymbol{R}_1\dot{\boldsymbol{x}}(v)\mathrm{d}v\mathrm{d}s \\ &\quad + (\bar{\tau} - \underline{\tau})\int_{t-\bar{\tau}}^{t-\underline{\tau}}\int_{s}^{t} \dot{\boldsymbol{x}}^{\mathrm{T}}(v)\boldsymbol{R}_2\dot{\boldsymbol{x}}(v)\mathrm{d}v\mathrm{d}s, \end{aligned}$$

$$V_4(t, \boldsymbol{x}_t) = (\bar{\tau} - \tau(t))\int_{t-\tau(t)}^{t} \dot{\boldsymbol{x}}^{\mathrm{T}}(s)\boldsymbol{H}\dot{\boldsymbol{x}}(s)\mathrm{d}s.$$

Taking the time derivative of $V(t, x_t)$ along the trajectory of system Eq. (9) yields:

$$\dot{V}_1(t, \boldsymbol{x}_t) = \dot{\boldsymbol{x}}^{\mathrm{T}}(t)\boldsymbol{P}\boldsymbol{x}(t) + \boldsymbol{x}^{\mathrm{T}}(t)\boldsymbol{P}\dot{\boldsymbol{x}}(t) \tag{13}$$

$$\begin{aligned} \dot{V}_2(t, \boldsymbol{x}_t) = & \boldsymbol{x}^{\mathrm{T}}(t)\boldsymbol{Q}_1\boldsymbol{x}(t) \\ & + \boldsymbol{x}^{\mathrm{T}}(t - \tau_1)(\boldsymbol{Q}_2 - \boldsymbol{Q}_1)\boldsymbol{x}(t - \tau_1) \\ & - \boldsymbol{x}^{\mathrm{T}}(t - \tau_2)\boldsymbol{Q}_2\boldsymbol{x}(t - \tau_2) \end{aligned} \tag{14}$$

$$\dot{V}_3(t, \boldsymbol{x}_t) \leqslant \underline{\tau}^2\dot{\boldsymbol{x}}^{\mathrm{T}}(t)\boldsymbol{R}_1\dot{\boldsymbol{x}}(t) - \underline{\tau}\int_{t-\underline{\tau}}^{t} \dot{\boldsymbol{x}}^{\mathrm{T}}(s)\boldsymbol{R}_1\dot{\boldsymbol{x}}(s)\mathrm{d}s$$

$$+(\bar{\tau}-\underline{\tau})^2\dot{\boldsymbol{x}}^{\mathrm{T}}(t)\boldsymbol{R}_2\dot{\boldsymbol{x}}(t)$$
$$-(\bar{\tau}-\underline{\tau})\int_{t-\tau_2}^{t-\tau_1}\dot{\boldsymbol{x}}^{\mathrm{T}}(s)\boldsymbol{R}_2\dot{\boldsymbol{x}}(s)\mathrm{d}s \quad (15)$$

$$\dot{V}_4(t,\boldsymbol{x}_t) \leqslant -\int_{t-\tau(t)}^{t}\dot{\boldsymbol{x}}^{\mathrm{T}}(s)\boldsymbol{H}\dot{\boldsymbol{x}}(s)\mathrm{d}s + (\bar{\tau}-\tau(t))\dot{\boldsymbol{x}}^{\mathrm{T}}(t)\boldsymbol{H}\dot{\boldsymbol{x}}(t) \quad (16)$$

By using Jessen's inequality to deal with integral items in Eq. (15), Eq. (17) and Eq. (18) can be obtained as

$$-\underline{\tau}\int_{t-\underline{\tau}}^{t}\dot{\boldsymbol{x}}^{\mathrm{T}}(s)\boldsymbol{R}_1\dot{\boldsymbol{x}}(s)\mathrm{d}s \leqslant -\begin{bmatrix}\boldsymbol{x}^{\mathrm{T}}(t) & \boldsymbol{x}^{\mathrm{T}}(t-\underline{\tau})\end{bmatrix}\begin{bmatrix}\boldsymbol{R}_1 & * \\ -\boldsymbol{R}_1 & \boldsymbol{R}_1\end{bmatrix}\begin{bmatrix}\boldsymbol{x}(t) \\ \boldsymbol{x}(t-\underline{\tau})\end{bmatrix}$$
$$= -\boldsymbol{x}^{\mathrm{T}}(t)\boldsymbol{R}_1\boldsymbol{x}(t) + \boldsymbol{x}^{\mathrm{T}}(t)\boldsymbol{R}_1\boldsymbol{x}(t-\underline{\tau}) + \boldsymbol{x}^{\mathrm{T}}(t-\underline{\tau})\boldsymbol{R}_1\boldsymbol{x}(t) - \boldsymbol{x}^{\mathrm{T}}(t-\underline{\tau})\boldsymbol{R}_1\boldsymbol{x}(t-\underline{\tau}) \quad (17)$$

$$-(\bar{\tau}-\underline{\tau})\int_{t-\bar{\tau}}^{t-\underline{\tau}}\dot{\boldsymbol{x}}^{\mathrm{T}}(s)\boldsymbol{R}_2\dot{\boldsymbol{x}}(s)\mathrm{d}s \leqslant -\frac{\bar{\tau}-\underline{\tau}}{\tau(t)-\underline{\tau}}[\boldsymbol{x}^{\mathrm{T}}(t-\underline{\tau})-\boldsymbol{x}^{\mathrm{T}}(t-\tau(t))]\boldsymbol{R}_2[\boldsymbol{x}(t-\underline{\tau})-\boldsymbol{x}(t-\tau(t))] - \frac{\bar{\tau}-\underline{\tau}}{\bar{\tau}-\tau(t)}[\boldsymbol{x}^{\mathrm{T}}(t-\tau(t))-\boldsymbol{x}^{\mathrm{T}}(t-\bar{\tau})]\boldsymbol{R}_2[\boldsymbol{x}(t-\tau(t))-\boldsymbol{x}(t-\bar{\tau})] \quad (18)$$

For a matrix $\boldsymbol{U}$ satisfying Eq. (10), Eq. (18) can be transformed into Eq. (19) by using Lemma 1.

$$-(\bar{\tau}-\underline{\tau})\int_{t-\bar{\tau}}^{t-\underline{\tau}}\dot{\boldsymbol{x}}^{\mathrm{T}}(s)\boldsymbol{R}_2\dot{\boldsymbol{x}}(s)\mathrm{d}s \leqslant -\begin{Bmatrix}\boldsymbol{x}^{\mathrm{T}}(t-\underline{\tau})\boldsymbol{R}_2\boldsymbol{x}(t-\underline{\tau}) \\ +\boldsymbol{x}^{\mathrm{T}}(t-\underline{\tau})(\boldsymbol{U}^{\mathrm{T}}-\boldsymbol{R}_2)\boldsymbol{x}(t-\tau(t)) \\ -\boldsymbol{x}^{\mathrm{T}}(t-\underline{\tau})\boldsymbol{U}^{\mathrm{T}}\boldsymbol{x}(t-\bar{\tau}) \\ +\boldsymbol{x}^{\mathrm{T}}(t-\tau(t))(\boldsymbol{U}-\boldsymbol{R}_2)\boldsymbol{x}(t-\underline{\tau}) \\ +\boldsymbol{x}^{\mathrm{T}}(t-\tau(t))(2\boldsymbol{R}_2-\boldsymbol{U}^{\mathrm{T}}-\boldsymbol{U})\boldsymbol{x}(t-\tau(t)) \\ +\boldsymbol{x}^{\mathrm{T}}(t-\tau(t))(\boldsymbol{U}^{\mathrm{T}}-\boldsymbol{R}_2)\boldsymbol{x}(t-\tau_2) \\ -\boldsymbol{x}^{\mathrm{T}}(t-\bar{\tau})\boldsymbol{U}\boldsymbol{x}(t-\underline{\tau}) \\ +\boldsymbol{x}^{\mathrm{T}}(t-\bar{\tau})(\boldsymbol{U}-\boldsymbol{R}_2)\boldsymbol{x}(t-\tau(t)) \\ +\boldsymbol{x}^{\mathrm{T}}(t-\bar{\tau})\boldsymbol{R}_2\boldsymbol{x}(t-\bar{\tau})\end{Bmatrix} \quad (19)$$

By using the Newton-Leibniz formula, and for a free weighting matrix $\hat{\boldsymbol{M}}$ with appropriate dimensions, it is clear that

$$2\boldsymbol{\xi}^{\mathrm{T}}(t)\hat{\boldsymbol{M}}[\boldsymbol{x}(t)-\boldsymbol{x}(t-\tau(t))-\int_{t-\tau(t)}^{t}\dot{\boldsymbol{x}}(s)\mathrm{d}s] = 0 \quad (20)$$

where $\boldsymbol{\xi}^{\mathrm{T}}(t) = [\boldsymbol{x}^{\mathrm{T}}(t) \quad \boldsymbol{x}^{\mathrm{T}}(t-\underline{\tau}) \quad \boldsymbol{x}^{\mathrm{T}}(t-\tau(t)) \quad \boldsymbol{x}^{\mathrm{T}}(t-\bar{\tau})]$.

Eq. (21) can be obtained by using Cauchy inequality.

$$-2\xi^{\mathrm{T}}(t)\hat{\boldsymbol{M}}\int_{t-\tau(t)}^{t}\dot{\boldsymbol{x}}(s)\mathrm{d}s \leqslant \tau(t)\xi^{\mathrm{T}}(t)\hat{\boldsymbol{M}}\boldsymbol{H}^{-1}\hat{\boldsymbol{M}}^{\mathrm{T}}\xi(t) + \int_{t-\tau(t)}^{t}\dot{\boldsymbol{x}}^{\mathrm{T}}(s)\boldsymbol{H}\dot{\boldsymbol{x}}(s)\mathrm{d}s \quad (21)$$

Combining Eqs (13) – (21), the following inequality can be obtained.

$$\dot{V}(t) \leqslant \xi^{\mathrm{T}}(t)\begin{bmatrix}\boldsymbol{\Xi}+\tau(t)\boldsymbol{M}\boldsymbol{H}^{-1}\boldsymbol{M}^{\mathrm{T}} \\ +2\boldsymbol{M}(\boldsymbol{e}_1-\boldsymbol{e}_3)+(\bar{\tau}-\tau(t))\boldsymbol{\Gamma}^{\mathrm{T}}(t)\boldsymbol{H}\boldsymbol{\Gamma}\end{bmatrix}\xi(t) \quad (22)$$

As $\tau_1 \leqslant \tau(t) \leqslant \tau_2$, and according to Lemma 2, when the conditions Eq. (11) and Eq. (12) in Theorem 1 are satisfied, there is

$$\begin{bmatrix}\boldsymbol{\Xi}+\tau(t)\boldsymbol{M}\boldsymbol{H}^{-1}\boldsymbol{M}^{\mathrm{T}} \\ +2\boldsymbol{M}(\boldsymbol{e}_1-\boldsymbol{e}_3)+(\bar{\tau}-\tau(\mathrm{t}))\boldsymbol{\Gamma}^{\mathrm{T}}(t)\boldsymbol{H}\boldsymbol{\Gamma}\end{bmatrix} < -\boldsymbol{e}_1^{\mathrm{T}}(\hat{\boldsymbol{Q}}+\boldsymbol{K}^{\mathrm{T}}\hat{\boldsymbol{R}}\boldsymbol{K})\boldsymbol{e}_1 \quad (23)$$

therefore

$$\dot{V}(t) \leqslant 0 \quad (24)$$

and the NCS Eq. (9) is asymptotically stable.

According to Eqs (22) – (24), there are $\dot{V}(t) \leqslant -\boldsymbol{x}^{\mathrm{T}}(t)(\hat{\boldsymbol{Q}}+\boldsymbol{K}^{\mathrm{T}}\hat{\boldsymbol{R}}\boldsymbol{K})\boldsymbol{x}(t)$, and

$$-V(0) = \int_0^{\infty}\dot{V}(t)\mathrm{d}t \leqslant -\int_0^{\infty}\boldsymbol{x}^{\mathrm{T}}(t)(\hat{\boldsymbol{Q}}+K^{\mathrm{T}}\hat{\boldsymbol{R}}\boldsymbol{K})\boldsymbol{x}(t)\mathrm{d}t = -\int_0^{\infty}\boldsymbol{x}^{\mathrm{T}}(t)\hat{\boldsymbol{Q}}\boldsymbol{x}(t)+\boldsymbol{u}^{\mathrm{T}}(t)\hat{\boldsymbol{R}}\boldsymbol{u}(t)\mathrm{d}t$$

Therefore, the cost function or performance index J has the upper bound.

$$J = \int_0^{\infty}(\boldsymbol{x}^{\mathrm{T}}(t)\hat{\boldsymbol{Q}}\boldsymbol{x}(t)+\boldsymbol{u}^{\mathrm{T}}(t)\hat{\boldsymbol{R}}\boldsymbol{u}(t)) < V(0)$$

The proof is thus completed.

2.3 LMI design conditions for networked PID control

Theorem 2 For some given constants $0 < \underline{\tau} < \bar{\tau}$, if there exist matrices $\boldsymbol{X} > 0$, $\boldsymbol{Y} > 0$, $\widetilde{\boldsymbol{Q}}_1 > 0$, $\widetilde{\boldsymbol{Q}}_2 > 0$, $\widetilde{\boldsymbol{R}}_1 > 0$, $\widetilde{\boldsymbol{R}}_2 > 0$, $\widetilde{\boldsymbol{H}} > 0$, $\widetilde{\boldsymbol{M}}$ and $\widetilde{\boldsymbol{U}}$ with appropriate dimensions satisfying the following matrix inequalities.

$$\begin{bmatrix}\widetilde{\boldsymbol{R}}_2 & * \\ \widetilde{\boldsymbol{U}} & \widetilde{\boldsymbol{R}}_2\end{bmatrix} > 0 \quad (25)$$

Define $\boldsymbol{X} = \boldsymbol{P}^{-1}$, $\boldsymbol{Y} = \boldsymbol{K}\boldsymbol{X}$, $\widetilde{\boldsymbol{Q}}_1 = \boldsymbol{X}\boldsymbol{Q}_1\boldsymbol{X}$, $\widetilde{\boldsymbol{Q}}_2 = \boldsymbol{X}\boldsymbol{Q}_2\boldsymbol{X}$, $\widetilde{\boldsymbol{R}}_1 = \boldsymbol{X}\widetilde{\boldsymbol{R}}_1\boldsymbol{X}$, $\widetilde{\boldsymbol{R}}_2 = \boldsymbol{X}\widetilde{\boldsymbol{R}}_2\boldsymbol{X}$, and $\widetilde{\boldsymbol{M}}_j = \boldsymbol{X}\boldsymbol{M}_j\boldsymbol{X}$, $1 \leqslant j \leqslant 5$. Then, pre- and post-multiplying both sides of Eq. (28) with $\mathrm{diag}\{\boldsymbol{P}^{-1}, \boldsymbol{P}^{-1}, \boldsymbol{P}^{-1}, \boldsymbol{P}^{-1}, \boldsymbol{P}^{-1}, \boldsymbol{R}_1^{-1}, \boldsymbol{R}_2^{-1}, \boldsymbol{H}^{-1}\}$ and its transpose respectively, Eq. (26) can be readily reached. Eq. (25) can be also obtained by pre- and post-multiplying both sides of Eq. (10) with $\mathrm{diag}\{\boldsymbol{X}, \boldsymbol{X}\}$ and its transpose respectively. Similarly, Eq. (27) can be obtained from Eq. (12). This completes the proof.

$$\begin{bmatrix}
\begin{pmatrix} \boldsymbol{X}\boldsymbol{A}^{\mathrm{T}} + \boldsymbol{A}\boldsymbol{X} + \widetilde{\boldsymbol{Q}}_1 \\ -\widetilde{\boldsymbol{R}}_1 + \widetilde{\boldsymbol{M}}_1 + \widetilde{\boldsymbol{M}}_1^{\mathrm{T}} \end{pmatrix} & * & * & * & * & * & * & * & & \\
\widetilde{\boldsymbol{R}}_1 + \widetilde{\boldsymbol{M}}_2 & \begin{pmatrix} \widetilde{\boldsymbol{Q}}_2 - \widetilde{\boldsymbol{Q}}_1 \\ -\widetilde{\boldsymbol{R}}_1 - \widetilde{\boldsymbol{R}}_2 \end{pmatrix} & * & * & * & * & * & * & * & * \\
(\boldsymbol{Y}^{\mathrm{T}}\boldsymbol{B}^{\mathrm{T}} + \widetilde{\boldsymbol{M}}_3 - \widetilde{\boldsymbol{M}}_1^{\mathrm{T}}) & \widetilde{\boldsymbol{R}}_2 - \widetilde{\boldsymbol{U}} - \widetilde{\boldsymbol{M}}_2^{\mathrm{T}} & \begin{pmatrix} -(2\widetilde{\boldsymbol{R}}_2 - \widetilde{\boldsymbol{U}}^{\mathrm{T}} - \widetilde{\boldsymbol{U}}) \\ -\widetilde{\boldsymbol{M}}_3 - \widetilde{\boldsymbol{M}}_3^{\mathrm{T}} \end{pmatrix} & * & * & * & * & * & * & * \\
\widetilde{\boldsymbol{M}}_4 & \widetilde{\boldsymbol{U}} & \widetilde{\boldsymbol{R}}_2 - \widetilde{\boldsymbol{U}} - \widetilde{\boldsymbol{M}}_4 & -\widetilde{\boldsymbol{Q}}_2 - \widetilde{\boldsymbol{R}}_2 & * & * & * & * & * & * \\
\sqrt{\tau}\widetilde{\boldsymbol{M}}_1^{\mathrm{T}} & \sqrt{\tau}\widetilde{\boldsymbol{M}}_2^{\mathrm{T}} & \sqrt{\tau}\widetilde{\boldsymbol{M}}_3^{\mathrm{T}} & \sqrt{\tau}\widetilde{\boldsymbol{M}}_4^{\mathrm{T}} & -\widetilde{\boldsymbol{H}} & * & * & * & * & * \\
\underline{\tau}\boldsymbol{A}\boldsymbol{X} & 0 & \underline{\tau}\boldsymbol{B}\boldsymbol{Y} & 0 & 0 & -\boldsymbol{X}\widetilde{\boldsymbol{R}}_1^{-1}\boldsymbol{X} & * & * & * & * \\
(\bar{\tau} - \underline{\tau})\boldsymbol{A}\boldsymbol{X} & 0 & (\bar{\tau} - \underline{\tau})\boldsymbol{B}\boldsymbol{Y} & 0 & 0 & 0 & -\boldsymbol{X}\widetilde{\boldsymbol{R}}_2^{-1}\boldsymbol{X} & * & * & * \\
\sqrt{(\bar{\tau} - \underline{\tau})}\boldsymbol{A}\boldsymbol{X} & 0 & \sqrt{(\bar{\tau} - \underline{\tau})}\boldsymbol{B}\boldsymbol{Y} & 0 & 0 & 0 & 0 & -\boldsymbol{X}\widetilde{\boldsymbol{H}}^{-1}\boldsymbol{X} & * & * \\
\hat{\boldsymbol{Q}}\boldsymbol{X} & 0 & 0 & 0 & 0 & 0 & 0 & 0 & -\hat{\boldsymbol{Q}}^{-1} & * \\
\hat{\boldsymbol{R}}\boldsymbol{Y} & 0 & 0 & 0 & 0 & 0 & 0 & 0 & 0 & -\hat{\boldsymbol{R}}^{-1}
\end{bmatrix} < 0 \tag{26}$$

$$\begin{bmatrix}
\begin{pmatrix} \boldsymbol{X}\boldsymbol{A}^{\mathrm{T}} + \boldsymbol{A}\boldsymbol{X} + \widetilde{\boldsymbol{Q}}_1 \\ -\widetilde{\boldsymbol{R}}_1 + \widetilde{\boldsymbol{M}}_1 + \widetilde{\boldsymbol{M}}_1^{\mathrm{T}} \end{pmatrix} & * & * & * & * & * & * & * & * \\
\widetilde{\boldsymbol{R}}_1 + \widetilde{\boldsymbol{M}}_2 & \begin{pmatrix} \widetilde{\boldsymbol{Q}}_2 - \widetilde{\boldsymbol{Q}}_1 \\ -\widetilde{\boldsymbol{R}}_1 - \widetilde{\boldsymbol{R}}_2 \end{pmatrix} & * & * & * & * & * & * & * \\
(\boldsymbol{Y}^{\mathrm{T}}\boldsymbol{B}^{\mathrm{T}} + \widetilde{\boldsymbol{M}}_3 - \widetilde{\boldsymbol{M}}_1^{\mathrm{T}}) & \widetilde{\boldsymbol{R}}_2 - \widetilde{\boldsymbol{U}} - \widetilde{\boldsymbol{M}}_2^{\mathrm{T}} & \begin{pmatrix} -(2\widetilde{\boldsymbol{R}}_2 - \widetilde{\boldsymbol{U}}^{\mathrm{T}} - \widetilde{\boldsymbol{U}}) \\ -\widetilde{\boldsymbol{M}}_3 - \widetilde{\boldsymbol{M}}_3^{\mathrm{T}} \end{pmatrix} & * & * & * & * & * & * \\
\widetilde{\boldsymbol{M}}_4 & \widetilde{\boldsymbol{U}} & \widetilde{\boldsymbol{R}}_2 - \widetilde{\boldsymbol{U}} - \widetilde{\boldsymbol{M}}_4 & -\widetilde{\boldsymbol{Q}}_2 - \widetilde{\boldsymbol{R}}_2 & * & * & * & * & * \\
\sqrt{\tau}\widetilde{\boldsymbol{M}}_1^{\mathrm{T}} & \sqrt{\tau}\widetilde{\boldsymbol{M}}_2^{\mathrm{T}} & \sqrt{\tau}\widetilde{\boldsymbol{M}}_3^{\mathrm{T}} & \sqrt{\tau}\widetilde{\boldsymbol{M}}_4^{\mathrm{T}} & -\widetilde{\boldsymbol{H}} & * & * & * & * \\
\underline{\tau}\boldsymbol{A}\boldsymbol{X} & 0 & \underline{\tau}\boldsymbol{B}\boldsymbol{Y} & 0 & 0 & -\boldsymbol{X}\widetilde{\boldsymbol{R}}_1^{-1}\boldsymbol{X} & * & * & * \\
(\bar{\tau} - \underline{\tau})\boldsymbol{A}\boldsymbol{X} & 0 & (\bar{\tau} - \underline{\tau})\boldsymbol{B}\boldsymbol{Y} & 0 & 0 & 0 & -\boldsymbol{X}\widetilde{\boldsymbol{R}}_2^{-1}\boldsymbol{X} & * & * \\
\hat{\boldsymbol{Q}}\boldsymbol{X} & 0 & 0 & 0 & 0 & 0 & 0 & -\hat{\boldsymbol{Q}}^{-1} & * \\
\hat{\boldsymbol{R}}\boldsymbol{Y} & 0 & 0 & 0 & 0 & 0 & 0 & 0 & -\hat{\boldsymbol{R}}^{-1}
\end{bmatrix} < 0 \tag{27}$$

Then the closed-loop NCS system Eq. (9) is asymptotically stable. Moreover, the delay-dependent controller gain can be obtained as $\boldsymbol{K} = \boldsymbol{Y}\boldsymbol{X}^{-1}$.

Poof Applying Schur complement to Eq. (11), it is easy to see that Eq. (28) is satisfied:

$$\begin{bmatrix}
\begin{pmatrix} \boldsymbol{A}^{\mathrm{T}}\boldsymbol{P} + {}^{\mathrm{T}}\boldsymbol{P}\boldsymbol{A} + \boldsymbol{Q}_1 \\ -\boldsymbol{R}_1 + \boldsymbol{M}_1 + \boldsymbol{M}_1^{\mathrm{T}} \end{pmatrix} & * & * & * & * & * & * & * & & \\
\boldsymbol{R}_1 + \boldsymbol{M}_2 & \begin{pmatrix} \boldsymbol{Q}_2 - \boldsymbol{Q}_1 \\ -\boldsymbol{R}_1 - \boldsymbol{R}_2 \end{pmatrix} & * & * & * & * & * & * & * & * \\
(\boldsymbol{K}^{\mathrm{T}}\boldsymbol{B}^{\mathrm{T}}\boldsymbol{P} + \boldsymbol{M}_3 - \boldsymbol{M}_1^{\mathrm{T}}) & \boldsymbol{R}_2 - \boldsymbol{U} - \boldsymbol{M}_2^{\mathrm{T}} & \begin{pmatrix} -(2\boldsymbol{R}_2 - \boldsymbol{U}^{\mathrm{T}} - \boldsymbol{U}) \\ -\boldsymbol{M}_3 - \boldsymbol{M}_3^{\mathrm{T}} \end{pmatrix} & * & * & * & * & * & * & * \\
\boldsymbol{M}_4 & \boldsymbol{U} & -(\boldsymbol{U} - \boldsymbol{R}_2) - \boldsymbol{M}_4 & -\boldsymbol{Q}_2 - \boldsymbol{R}_2 & * & * & * & * & * & * \\
\sqrt{\underline{\tau}}\boldsymbol{M}_1^{\mathrm{T}} & \sqrt{\underline{\tau}}\boldsymbol{M}_2^{\mathrm{T}} & \sqrt{\underline{\tau}}\boldsymbol{M}_3^{\mathrm{T}} & \sqrt{\underline{\tau}}\boldsymbol{M}_4^{\mathrm{T}} & -\boldsymbol{H} & * & * & * & * & * \\
\underline{\tau}\boldsymbol{A} & 0 & \underline{\tau}\boldsymbol{B}\boldsymbol{K} & 0 & 0 & -\boldsymbol{R}_1^{-1} & * & * & * & * \\
(\bar{\tau} - \underline{\tau})\boldsymbol{A} & 0 & (\bar{\tau} - \underline{\tau})\boldsymbol{B}\boldsymbol{K} & 0 & 0 & 0 & -\boldsymbol{R}_2^{-1} & * & * & * \\
\sqrt{(\bar{\tau} - \underline{\tau})}\boldsymbol{A} & 0 & \sqrt{(\bar{\tau} - \underline{\tau})}\boldsymbol{A} & 0 & 0 & 0 & 0 & -\boldsymbol{H}^{-1} & * & * \\
\hat{\boldsymbol{Q}} & 0 & 0 & 0 & 0 & 0 & 0 & 0 & -\hat{\boldsymbol{Q}}^{-1} & * \\
\hat{\boldsymbol{R}}\boldsymbol{K} & 0 & 0 & 0 & 0 & 0 & 0 & 0 & 0 & -\hat{\boldsymbol{R}}^{-1}
\end{bmatrix}$$

< 0 (28)

Note that the conditions in Theorem 2 includes nonlinear terms, such as $\boldsymbol{X}\widetilde{\boldsymbol{R}}_1^{-1}\boldsymbol{X}$, $\boldsymbol{X}\widetilde{\boldsymbol{R}}_2^{-1}\boldsymbol{X}$, $\boldsymbol{X}\boldsymbol{H}^{-1}\boldsymbol{X}$. First of all, assume that the matrixes $\boldsymbol{L}_1 > 0$, $\boldsymbol{L}_2 > 0$, $\boldsymbol{L}_3 > 0$ satisfies

$$-\boldsymbol{L}_3 \geqslant -\boldsymbol{X}\widetilde{\boldsymbol{H}}^{-1}\boldsymbol{X},\ -\boldsymbol{L}_i \geqslant -\boldsymbol{X}\widetilde{\boldsymbol{R}}_i^{-1}\boldsymbol{X} \quad i = 1,2 \tag{29}$$

Then Eq. (30) can be obtained by using Schur complement from Eq. (29).

$$\begin{bmatrix} -\widetilde{\boldsymbol{H}}^{-1} & \boldsymbol{X}^{-1} \\ \boldsymbol{X}^{-1} & -\boldsymbol{L}_3^{-1} \end{bmatrix} \leqslant 0,\ \begin{bmatrix} -\widetilde{\boldsymbol{R}}_i^{-1} & \boldsymbol{X}^{-1} \\ \boldsymbol{X}^{-1} & -\boldsymbol{L}_i^{-1} \end{bmatrix} \leqslant 0 \quad i = 1,2 \tag{30}$$

By introducing new variables $\boldsymbol{X}_N$, $\boldsymbol{R}_{1N}$, $\boldsymbol{R}_{2N}$, $\boldsymbol{L}_{1N}$, $\boldsymbol{L}_{2N}$, Eq. (30) can be rewritten as

$$\begin{bmatrix} -\widetilde{\boldsymbol{H}}_N & \boldsymbol{X}_N \\ \boldsymbol{X}_N & -\boldsymbol{L}_{3N} \end{bmatrix} \leqslant 0, \begin{bmatrix} -\widetilde{\boldsymbol{R}}_{iN} & \boldsymbol{X}_N \\ \boldsymbol{X}_N & -\boldsymbol{L}_{iN} \end{bmatrix} \leqslant 0 \quad i = 1,2 \tag{31}$$

where $\boldsymbol{X}\boldsymbol{X}_N = \boldsymbol{I}$, $\widetilde{\boldsymbol{R}}_1\widetilde{\boldsymbol{R}}_{1N} = \boldsymbol{I}$, $\widetilde{\boldsymbol{R}}_2\widetilde{\boldsymbol{R}}_{2N} = \boldsymbol{I}$, $\widetilde{\boldsymbol{H}}\widetilde{\boldsymbol{H}}_N = \boldsymbol{I}$, $\boldsymbol{L}_1\boldsymbol{L}_{1N} = \boldsymbol{I}$, $\boldsymbol{L}_2\boldsymbol{L}_{2N} = \boldsymbol{I}$ and $\boldsymbol{L}_3\boldsymbol{L}_{3N} = \boldsymbol{I}$. Therefore, the nonlinear terms in Theorem 2 could be changed to a minimization problem subject to LMIs and could be solved by using the modified cone complementarity linearization (CCL) algorithms in Ref. [25].

3 Experiment

Considering NCSs with bilateral time-varying delay and packet dropouts, the effectiveness of the proposed approach for networked guaranteed cost PID attitude tracking control of a 3-DOF helicopter is illustrated in this section. To build the model, actual 3-DOF helicopter parameters in Table 1 can be used.

The block diagram of experimental system, and the actual experimental system are shown in Fig. 7 and Fig. 8, respectively. PC1, as the actuator and sensor (acquisition card), communicates with the controller (PC2) through different network ports. As shown in Fig. 7, the PC1 is connected to the LANs of the laboratory through the network cable, while PC2 is connected to the router through WiFi. In order to facilitate the implementation of the experimental system, the UDP communication protocol are adopted. The network delay between PC1 and PC2 can be estimated by Ping command, which is almost all distributed below 20 ms.

Assuming the sampling period is h, the network induced delays interval is $\tau_k \in (0, h)$. $\underline{\tau} = 0$ ms and

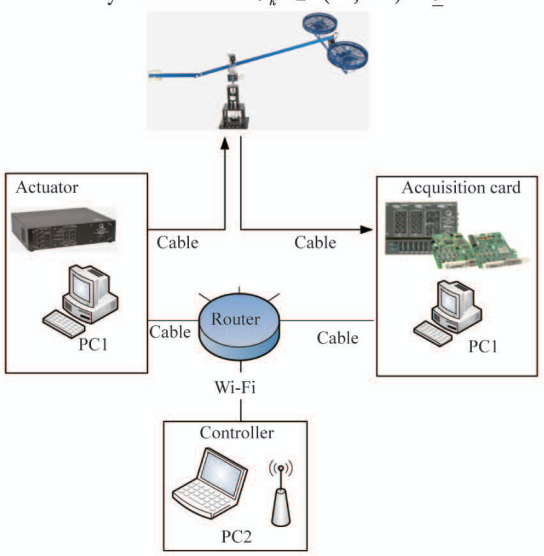

Fig. 7 The block diagram of experimental system

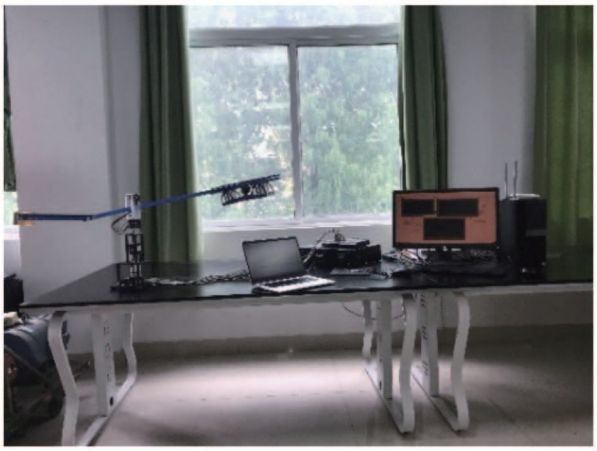

Fig. 8 The actual experimental system

$\overline{\tau} = 160$ ms are considered. By using Theorem 2, the performance of specific states and control sequence can be controlled by adjusting $\hat{\boldsymbol{Q}}$ and $\hat{\boldsymbol{R}}$, respectively.

By selecting the reasonable weight matrices $\hat{\boldsymbol{Q}}$ and $\hat{\boldsymbol{R}}$, it is possible to make tradeoffs between the inputs and system state performance by using a linear quadratic regulation approach. However, there is no general rule about the choice of $\hat{\boldsymbol{Q}}$ and $\hat{\boldsymbol{R}}$. Thus, it should resort to trial and error to get reasonable values. After resorting to trial and error, and simulations, the weighting matrices can be chosen as

$$\hat{\boldsymbol{Q}} = \mathrm{diag}\begin{pmatrix} 1, 0.8, 1, 1 \times 10\hat{}(-5), 1 \times 10\hat{}(-5), \\ 0.5 \times 10\hat{}(-5), 1.5 \times 10\hat{}(2), 5 \end{pmatrix},$$

$$\hat{\boldsymbol{R}} = \mathrm{diag}(1, 1)$$

and the corresponding controller gain can be obtained.

$$\boldsymbol{K} = \begin{bmatrix} -15.1982 & -6.4354 & 4.3784 & -13.2680 \\ -15.1982 & 6.4354 & -4.3784 & -13.2680 \\ -3.2412 & 6.0808 & -8.6241 & \\ 3.2412 & -6.0808 & -8.6241 & \end{bmatrix}$$

Then, it is dedicated to illustrate the tuning of the networked guaranteed cost PID based on the control gain $\boldsymbol{K}$, which is obtained by solving the matrix inequalities in Theorem 2.

As $\boldsymbol{u}(t) = [U_f \quad U_b]^{\mathrm{T}} = \boldsymbol{K}\boldsymbol{x}(t)$, the following Eq. (32) can be obtained from the gain $\boldsymbol{K}$.

$$U_f + U_b = 2k_{11}\varepsilon + 2k_{14}\dot{\varepsilon} + 2k_{17}\int \varepsilon \mathrm{d}t \tag{32}$$

Considering the schematic of networked tracking control for a 3-DOF helicopter in Fig. 6, the elevation control Eq. (33) is

$$V_s = 2k_{11}\varepsilon_e + 2k_{14}\dot{\varepsilon}_e + 2k_{17}\int \varepsilon_e \mathrm{d}t \tag{33}$$

Similar to Eq. (33), the difference of U_f and U_b can be also obtained as

$$U_f - U_b = 2k_{12}\rho + 2k_{13}\lambda + 2k_{15}\dot{\rho} + 2k_{16}\dot{\lambda} + 2k_{18}\int \lambda \mathrm{d}t \tag{34}$$

and the pitch control equation in Fig. 6 can be expressed as

$$V_d = 2k_{12}\rho + 2k_{15}\dot{\rho} + 2k_{13}\lambda_e + 2k_{16}\dot{\lambda}_e + 2k_{18}\int\lambda_e \mathrm{d}t \tag{35}$$

Define $\rho_d = \dfrac{1}{2k_{12}}(2k_{13}\lambda_e + 2k_{16}\dot{\lambda}_e + 2k_{18}\int\lambda_e \mathrm{d}t)$ is the desired pitch angle, which results in the desired travel angle. Thus, the desired pitch angle ρ_d needs to be designed to achieve the desired travel angle λ_d by the following controller Eq. (36).

$$V_d = 2k_{12}(\rho - \rho_d) + 2k_{15}\dot{\rho} \tag{36}$$

Obviously, Eq. (33), Eq. (35) and Eq. (36) achieve the PID control equation in Section 2.1 according to the obtained control gain $\boldsymbol{K}$.

In sequence, the problem of tracking desired reference trajectories for elevation and travel angles is investigated. The desired reference signals are given by

$$\varepsilon_d(s) = \frac{1}{s+1}w_\varepsilon(s),\ \lambda_d(s) = \frac{1}{3s+1}w_\lambda(s) \tag{37}$$

where $w_i(s)$, $(i = \varepsilon, \lambda)$ denotes the reference input commands of the elevation and travel angles, respectively. The desired reference signals are defined in Eq. (37), for desired elevation angle, the reference input command is a square waveform reference signal with amplitude of $0 - 15°$ and frequency 0.015 Hz. For desired travel angle, a wave with amplitude $\pm 20°$ and frequency 0.01 Hz. And the desired pitch angle is kept to be 0.

As $\underline{\tau} = 0$ ms and $\overline{\tau} = 160$ ms, so when the sensor sampling period $h = 80$ ms is taken into account, the packet dropouts will not be considered in the first case. When the sensor sampling period is set to 40 ms, the maximum number 2 of consecutive packet dropouts can be set in the second case, and the packet dropouts sequence is set to $\cdots 0010010011 \cdots 0010010011$ (where 0 represents no packet dropouts, while 1 represents packet dropouts), then the packet dropouts rate reaches 40%. In addition, the PID controller uses the sensor sampling cycle time for discretization in the experiment.

In order to better verify the effectiveness of the proposed algorithm, in addition to considering the delay of the network itself, the delay in the range of 0 – 60 ms and 0 – 20 ms are artificially added at the controller (PC2) in the 2 cases, respectively.

For above 2 cases, Fig. 9 and Fig. 10 show the responses of elevation, travel and pitch angle, respectively. It can be seen that the system can track the input elevation and travel attitude signals as well as expected. In addition, the fluctuation of pitch angle is relatively small, which is consistent with the hypothesis in Section 2.

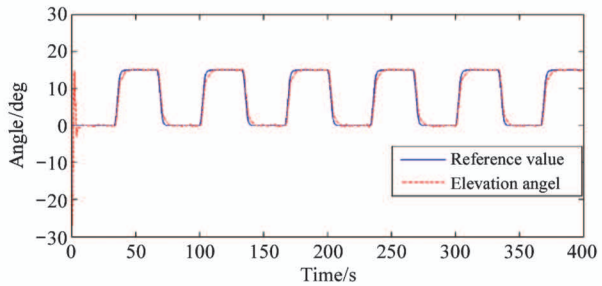

(a) Response of the elevation angle

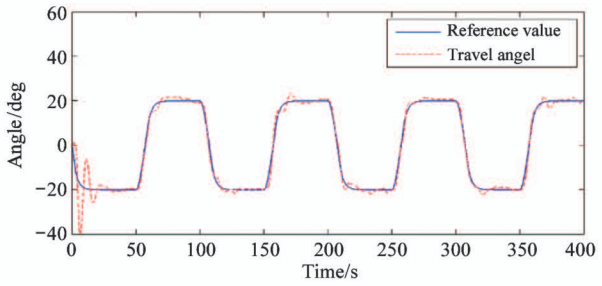

(b) Response of the travel angle

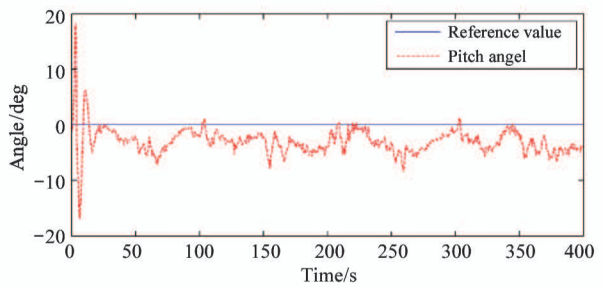

(c) Response of the pitch angle

Fig. 9 Responses of tracking reference signals for case 1

4 Conclusions

The networked guaranteed cost PID attitude tracking control of a 3-DOF helicopter has been proposed. Considering the 3-DOF helicopter characteristics of MIMO, channel coupling and nonlinearity, a linear state space model is established by analyzing the motions on elevation, pitch, and travel axis. Furthermore, a linear time delay system is modeled with consideration of the time-varying delay and packet dropouts in communication network. Based on the reciprocal convex approach, the free weight matrix, and CCL method, the PID tracking controller parameters, which satisfy the tracking performance, can be obtained by solving the related linear matrix inequalities. At the end of the paper, a practical experiment of laboratory 3-DOF helicopter is given to illustrate the effectiveness of the proposed method.

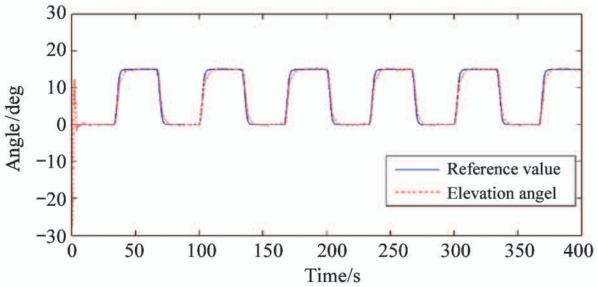

(a) Response of the elevation angle

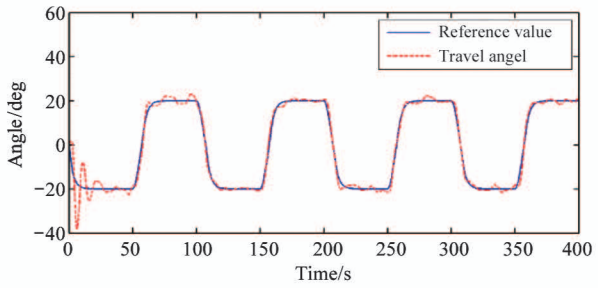

(b) Response of the travel angle

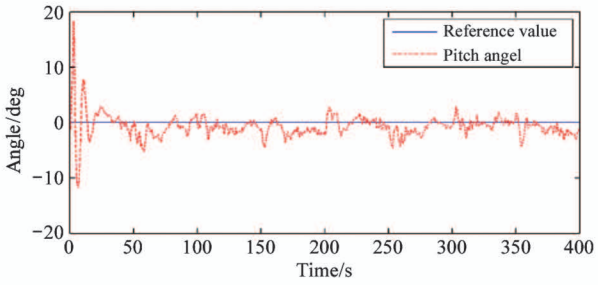

(c) Response of the pitch angle

Fig. 10 Responses of tracking reference signals for case 2

References

[1] Pérez-Ventura U, Fridman L, Capello E, et al. Fault tolerant control based on continuous twisting algorithms of a 3-DoF helicopter prototype [J]. *Control Engineering Practice*, 2020, 101: 104486

[2] Mehndiratta M, Kayacan E. Receding horizon control of a 3 DOF helicopter using online estimation of aerodynamic parameters[J]. *Proceedings of the Institution of Mechanical Engineers, Part G: Journal of Aerospace Engineering*, 2017, 232(8):1442-1453

[3] Chen M, Shi P, Lim C C. Adaptive neural fault-tolerant control of a 3-DOF model helicopter system [J]. *IEEE Transactions on Systems Man and Cybernetics Systems*, 2016, 46(2):260-270

[4] Liu H, Lu G, Zhong Y. Robust LQR attitude control of a 3-DOF laboratory helicopter for aggressive maneuvers[J]. *IEEE Transactions on Industrial Electronics*, 2013, 60(10):4627-4636

[5] Li D, Zhu X, Li W, et al. Experimental results on robust attitude control of a 3-DOF helicopter under wind disturbances[C]//2019 Chinese Control Conference (CCC), Guangzhou, China, 2019: 8824-8828

[6] Zhang J, Cheng X, Zhu J. Control of a laboratory 3-DOF helicopter: explicit model predictive approach[J]. *International Journal of Control Automation and Systems*, 2016, 14(2):389-399

[7] Huang Y J, Kuo T C, Way H K. Robust vertical takeoff and landing aircraft control via integral sliding mode[J]. *IEE Proceedings-Control Theory and Applications*, 2003, 150(4):383-388

[8] Castañeda H, Plestan F, Chriette A, et al. Continuous differentiator based on adaptive second-order sliding-mode control for a 3-DOF helicopter[J]. *IEEE Transactions on Industrial Electronics*, 2016, 63(9):5786-5793

[9] López-Martínez M, Ortega M G, Vivas C, et al. Nonlinear L2 control of a laboratory helicopter with variable speed rotors[J]. *Automatica*, 2007, 43(4): 655-661

[10] Vilchis J C A, Brogliato B, Dzul A, et al. Nonlinear modelling and control of helicopters [J]. *Automatica*, 2003, 39(9):1583-1596

[11] Kadmiry B, Driankov D. A fuzzy gain-scheduler for the attitude control of an unmanned helicopter [J]. *IEEE Transactions on Fuzzy Systems*, 2012, 12(4): 502-515

[12] Raptis I A, Valavanis K P, Moreno W A. A novel nonlinear backstepping controller design for helicopters using the rotation matrix[J]. *IEEE Transactions on Control Systems Technology*, 2011,19(2):465-473

[13] Prempain E, Postlethwaite I. Static H∞ loop shaping control of a fly-by-wire helicopter[J]. *Automatica*, 2005, 41(9):1517-1528

[14] Li M, Chen Y. Challenging research for networked control systems: a survey[J]. *Transactions of the Institute of Measurement and Control*, 2019,41(9),2400-4218

[15] Zhang X M, Han Q L, Ge X, et al. Networked control systems: a survey of trends and techniques[J]. *IEEE/CAA Journal of Automatica Sinica*, 2020, 7(1): 1-17

[16] Li M, Chen Y. A wide-area dynamic damping controller based on robust H∞ control for wide-area power systems with random delay and packet dropout[J]. *IEEE Transactions on Power Systems*, 2018, 33(4): 4026-4037

[17] Zhang D, Shi P, Wang Q G, et al. Analysis and synthesis of networked control systems: a survey of recent advances and challenges[J]. *ISA Transactions*, 2017, 66: 376-392

[18] Qiu Z Z, Li S F. Modeling and simulation of PID networked control systems based on neural network [J]. *Journal of System Simulation*, 2018, 30(4):1423-1432

[19] Tran H D, Guan Z H, Dang X K, et al. A normalized PID controller in networked control systems with varying time delays[J]. *ISA Transactions*, 2013, 52(5):592-599

[20] Ahmadi A A, Salmasi F R, Noori-Manzar M, et al. Speed sensorless and sensor-fault tolerant optimal PI regulator for networked DC motor system with unknown time-delay and packet dropout[J]. *IEEE Transactions on Industrial Electronics*, 2013, 61(2):708-717

[21] Zhang H, Shi Y, Mehr A S. Robust static output feedback control and remote PID design for networked motor systems[J]. *IEEE Transactions on Industrial Electronics*, 2011, 58(12):5396-5405

[22] Zhang H, Shi Y, Mehr A S. Robust H∞ PID control for multivariable networked control systems with disturbance/noise attenuation[J]. *International Journal of Robust and Nonlinear Control*, 2012, 22(2):183-204

[23] Park P G, Ko J W, Jeong C. Reciprocally convex approach to stability of systems with time-varying delays [J]. *Automatica*, 2011, 47(1):235-238

[24] Tian E, Yue D, Zhang Y. Delay-dependent robust H ∞, control for T-S fuzzy system with interval time-varying delay [J]. *Fuzzy Sets and Systems*, 2009, 160 (12):1708-1719

[25] He Y, Wu M, Liu G P, et al. Output feedback stabilization for a discrete time system with a time-varying delay [J]. *IEEE Transactions on Automatic Control*, 2008, 53 (10):2372-2377

Liu Yicai, born in 1982. He is currently pursuing the Ph. D degree at Wuhan University of Science and Technology, Wuhan, China. He received the B. S. degree in communication engineering from China University of Geosciences, Wuhan, China, in 2005, and M. S. degree from Institute of Modern Physics, Chinese Academy of Sciences, Lanzhou, China, in 2008. His research focuses on networked control systems and predictive control.